THE JOURNAL OF PHYSICAL CHEMISTRY C
A JOURNAL OF THE AMERICAN CHEMICAL SOCIETY

pubs.acs.org/JPCC

Article

Insight into SEI Growth in Li-Ion Batteries using Molecular Dynamics and Accelerated Chemical Reactions

Lorena Alzate-Vargas,* Samuel M. Blau, Evan Walter Clark Spotte-Smith, Srikanth Allu, Kristin A. Persson, and Jean-Luc Fattebert

Cite This: https://doi.org/10.1021/acs.jpcc.1c04149

Read Online

ACCESS | Metrics & More | Article Recommendations | Supporting Information

ABSTRACT: The performance of lithium-ion batteries (LIB) using organic electrolytes strongly depends on the formation of a stable solid electrolyte interphase (SEI) film. Elucidating the dynamic evolution and spatial composition of the SEI can be very useful to study the stability of SEI components and help optimize the formation cycles of LIB. We propose a classical molecular dynamics simulation protocol for predicting the first stages of SEI formation using a reaction method involving the decomposition of EC and $LiPF_6$ molecules in the electrolyte. We accelerate the formation of SEI components near the anode surface by increasing the probability of reactions, implemented through a geometry matching scheme, followed by a force-field reconfiguration. We observe the formation of gases (C_2H_4), inorganic (Li_2CO_3 and LiF) and organic (LEDC) components. This protocol shows promise to be able to evaluate the effects of varying electrolyte compositions and additives on SEI layer structure and composition.

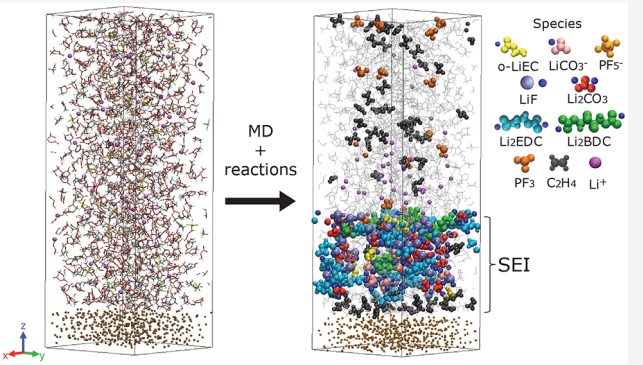

1. INTRODUCTION

Lithium-ion batteries (LIBs) are key for transforming the energy infrastructure and transportation toward the storage of renewable electricity and enabling long-range electrical vehicles. LIBs have been widely used in an extensive range of applications from small portable devices to large-scale energy storage systems.[1,2] The solid electrolyte interphase (SEI) is one of the most critical components due to its influence on the battery performance, that is, capacity degradation, safety, calendar life, and cycle life.[3−5] At the same time, it is the least understood component of lithium-ion batteries. The SEI usually consists of reduction products formed through reactions between an electrode and electrolyte due to the electron leakage from the anode.[6] The SEI layer can be viewed as a multilayered structure, an inorganic inner layer near the electrode that allows lithium ion transport and an organic outer layer permeable to electrolyte solvent molecules.[7] Numerous experimental techniques have been developed to characterize the film composition and contribute to an understanding of the SEI formation.[8,9] Nevertheless, fully characterizing the SEI remains a challenge. Still, the development of computational models that can contribute to its understanding have become more popular during the last years.[10,11] These techniques can unveil the details of SEI formation at a molecular level, providing insights that cannot be obtained from experiment alone.

Atomistic level studies using first-principles calculations have been able to predict the reductive reaction mechanism of ethylene carbonate (EC) and reaction pathways to multiple SEI components, such as LEDC.[12−14] Similarly, first-principles molecular dynamics (FPMD) studies have focused on the reductive decomposition mechanisms of electrolyte solvent molecules on different electrodes.[15−20] Although FPMD can predict chemistry, this includes the atom's electronic structure and can properly describe atomic bonds and forces, allowing bond breaking and bond formation, it is restricted to small systems and time resolution remains limited on the tens of picoseconds in practice. That drastically reduces the number of chemical reactions one can observe and would provide limited information about the SEI growth mechanism.

Classical molecular dynamics (MD) have become more popular to investigate the behavior of LIBs, since they allow simulations with bigger systems on nanosecond time scales. In general, such MD simulations do not allow reactive events, limiting their utility for studies of the SEI. Still, they have enabled simulations that capture the transport and structural

Received: May 10, 2021
Revised: August 6, 2021

properties of the electrolyte and SEI[21−25] and lead to an accurate description of the properties of the main SEI components.[26,27] Some MD simulations have modeled electrode−electrolyte structural changes under electric field, ignoring any chemical reactions or buildup of the SEI.[28−30] On the other hand, MD simulations accounting for reactivity with a reactive force field (ReaxFF) can calculate bond breaking/bond forming events. They have been used to investigate the pathways and activation energies of the reduction reactions of EC solvent molecules in LIB.[31,32] Some simulations have elucidated certain aspects of the SEI buildup on Li-metal and silicon based anodes, capturing the electrolyte decomposition but on a very short time scale (hundreds of picoseconds), more limited than nonreactive force-field simulations can achieve.[33−35] While ReaxFF can predict reactions on the fly, based on the dynamic evolution of the system, it requires the parametrization of all the atomic interactions in the system, limiting its applicability. Recently, Takenaka and co-workers[36] employed a hybrid MC/MD method to study the SEI formation mechanism on lithium- and sodium-ion batteries demonstrating the impact of larger and longer space-time scale simulations to understand complex chemical reaction processes. It is noted that their simulations are limited to a small set of predefined chemical reactions that occur based on a interatomic distance, whereas our simulations allow the specification of additional geometry constrains.

Given the importance of the SEI in lithium-ion batteries, improved molecular level understanding of SEI structure and Li ion transport can help design novel solvents and/or additives that would form SEIs with enhanced transport properties and increased voltage stability windows. Our goal is to develop a methodology that helps us understand SEI formation at the atomistic level, using classical MD simulations, by growing the SEI one molecule at a time, simulating the most relevant chemical reactions occurring within the electrolyte near the anode. MD simulations give us in particular a spatial component that continuum methodologies cannot determine, useful for designing SEI layers with improved properties.[11] In reality, chemical reactions are based on atomistic configurations, not only concentrations. Achieving this goal is however quite challenging. First of all, the time scale needed to simulate all of these chemical reactions is typically way beyond the time scales reached even by classical MD. To properly model the atomic vibrations in an MD calculation, a step on the femtosecond time scale is required. On the other hand, chemical reactions happen on a pico/nanosecond time scale, and the SEI growth occurs on a much longer time. To overcome this time-scale challenge, we have developed a strategy to accelerate reactive classical molecular dynamics simulations and simulate hundreds or even thousands of chemical reactions within the electrolyte. Our approach resembles the one proposed by Takenaka et al.[36] but with a richer set of chemical reactions as well as a more sophisticated algorithm to capture reactions based on the recent work of Gissinger et al.[37,38] Our work also differs in the way we handle the flow of lithium ions in the electrolyte and through the anode.

In this article, we present an atomistic MD simulation methodology, useful to investigate the early stages of SEI formation, described in Section 2. We used this protocol to predict the SEI growth for an EC-based electrolyte. Our results are in concordance with the existing literature and can be found in Section 3, followed by concluding remarks in Section 4.

2. METHODS

2.1. Model Systems. As illustrated in Figure 1, simulations were conducted using a system representing a half-cell (anode side) of a LIB; the rectangular simulation cell is comprised of a liquid electrolyte, 1 M $LiPF_6$ in EC, and a nonreactive amorphous silicon electrode.

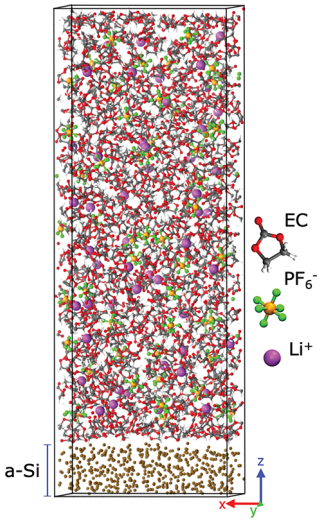

Figure 1. Simulation cell snapshot comprising 700 EC and 52 Li^+−PF_6^- pairs and an amorphous silicon anode (ochre).

An amorphous silicon (a-Si) slab of size of 32.58 Å × 32.58 Å × 8 Å, was created first using the melt-quench method and further relaxed for 2 ns at 298 K. An initial electrolyte system consisting of 350 EC molecules, 26 salt and Li^+molecules and 26 Li ions randomly packed in a periodic cubic box of size 32 Å × 32 Å × 32 Å was generated using packmol.[39] The simulation domain was then replicated along the *z*-direction, doubling the number of molecules in the system. The energy of the latter configuration was minimized by a conjugated-gradient minimization scheme, followed by an equilibration with periodic boundary conditions (PBC) applied in *x*- and *y*-directions, for 2 ns in the isothermal−isobaric (NPT) ensemble at a pressure of 1 atm and a temperature of 298 K with a time constant of 1 ps. An annealing process was conducted using the canonical ensemble (NVT), and the electrolyte was heated from 298 to 400 K for 1 ns, maintained at 400 K for 1 ns, and subsequently annealed from 400 to 298 K in 1 ns. Subsequently, the simulation box was deformed to a final size of 32.58 Å in both *x*- and *y*-directions, in order to match the size of the silicon electrode, followed by a relaxation in the *z*-direction for 1 ns at 298 K. The final electrolyte density is 1.32 g/cm^3, in good agreement with the experimental value.[4] Finally, the electrode/electrolyte system was relaxed for 1 ns in the canonical ensemble (NVT) under a Nose−Hoover thermostat at 298 K and periodic boundary conditions were used in all directions.

2.2. MD Reaction Method. To investigate the reaction processes that lead to the SEI formation, we have employed the REACTER algorithm,[37,38] implemented in the large-scale atomic/molecular massively parallel simulator (LAMMPS) code[40] as fix bond/react. As pointed out before, one strong

https://doi.org/10.1021/acs.jpcc.1c04149
J. Phys. Chem. C XXXX, XXX, XXX−XXX

Table 1. Set of Electrolyte Decomposition Reaction Used in Our Simulation[a]

	reaction	reaction constraints[b]	freq	prob
EC	$Li^+ + EC \rightleftharpoons Li^+(EC)$	1 distance (Oc−Li^+)	400	0.4
				0.6[c]
	$Li^+(EC) + e^- \rightarrow$ o-LiEC	1 distance (Oe−Li^+) & 1 angle (Oc−Cc−Oe)	200	0.4
	2(o-LiEC) → $Li_2EDC + C_2H_4 \uparrow$	1 distance (Oe_1-C_2)[d]	50	1
	2(o-LiEC) → Li_2BDC	1 distance (C_1-C_2)[d]	50	1
	o-LiEC + $e^- \rightarrow$ o-$LiEC^-$	1 distance (Cc−Li^+)	400	0.5
	o−$LiEC^- \rightarrow LiCO_3^- + C_2H_4 \uparrow$	1 distance (O−Li^+)	2000	1
	$LiCO_3^- + Li^+ \rightarrow Li_2CO_3$	1 distance (O−Li_+)	50	1
	$LiCO_3^- + Li^+(EC) \rightarrow Li_2EDC$	1 distance (O_1-C_2)[d]	50	1
PF_6^-	$PF_6^- + Li^+ + e^- \rightarrow PF_5^- + LiF \downarrow$	1 distance (F−Li^+)[e]	200	1
	$PF_5^- + Li^+ + e^- \rightarrow PF_4^- + LiF \downarrow$	1 distance (F−Li^+)[e]	50	1
	$PF_4^- + Li^+ \rightarrow PF_3 + LiF \downarrow$	1 distance (F−Li^+)[e]	50	1

[a]Also shown are the constraint types used for the REACTER protocol as well as the frequencies at which reaction templates are checked (in a number of steps) and the probabilities associated with each reaction. [b]Oc, carbonyl oxygen; Cc, carbonyl carbon; Oe, ether oxygen. [c]Probability for reversible reaction ($Li^+(EC) \rightarrow Li^+ + EC$). [d]Involves one atom from molecule 1 and one from molecule 2. [e]Any F atom in PF_x^-.

limitation with classical MD simulations is that nonreactive force fields do not allow chemical reactions to happen and reactive potential development is quite difficult. To overcome this restriction, one can identify when a chemical reaction is about to happen and explicitly restart the MD simulation with different atomic potential parameters and potential function forms, that describe the reaction products.

In the present study, we have included a set of reactions involving ethylene carbonate reduction and PF_6^- reduction process based on both previous experiments and theoretical studies.[13,41−45] The set of reactions shown in Table 1 leads to the formation of the various key SEI components detected experimentally, such as Li_2EDC, Li_2CO_3, and LiF.[46−50]

In order to carry out a reaction, the REACTER protocol consists of the following processes: (i) Search for potential reaction by checking that the distance between reaction site atoms is below the specified cutoff distance; (ii) for reaction sites that satisfy that condition, a matching algorithm compares the configuration of the reaction site and its surroundings at that time step with a prereaction template; (iii) the reaction is carried out if matching is successful. Every reaction requires the specification of prereaction (reactants) and postreaction (products) templates. They contain not only the geometry and atomic charges of the reactants but also the force field information, such that when a chemical reaction occurs, atomic potential parameters in the reactant molecules are replaced by those of the product.

Additional reaction constraints such as interatomic distances or angles can be specified in the templates and must be satisfied for a prereaction topology to be converted into a postreaction topology. It is important to mention that this differs from the approach of Takenaka et al.[36] where the geometry of the reactants is ignored and only interatomic distances are used.

Two extra arguments are specified for each reaction: (i) frequency, that is, the number of timesteps between checks for potential reactive sites, and (ii) the probability of an eligible reaction occurring. The probability can be tuned for different reaction pathways to proceed from the same reaction sites. In principle we could use actual reaction rates for the probabilities but that would require accurate and reliable data which is hard to obtain. Also, these rates would need to be rescaled to accelerate the products formation. In our simulation setup, the choice of these parameters was subsequent to the need of accelerating the reactions rates while conserving a reasonable overall behavior of the system, that is, we observe the formation of the expected SEI components. We use a baseline frequency of 50 timesteps, given the high correlation between consecutive MD timesteps, and a probability of 1. Variations to these numbers will be explained in Section 2.2.1. For each reaction listed in Table 1, we specify the type of constraints to be met, the template-matching frequency for the REACTER algorithm, and probability to initiate a reaction. More detailed information about the reaction templates can be found in the Supporting Information. It should be noted that the reactions implemented in our simulations can occur in any order.

For simplicity, the silicon anode is kept fixed during the reaction scheme, however it is crucial to our simulations since it acts as a barrier and a guide to as where reactions can occur. Reduction reactions are constrained to occur only in a finite redox region near the silicon electrode. We initially set a region of 5 Å, then let it evolve with time, growing each 5 ns and reaching a thickness of 15 Å after 90 ns. Since electrons are not explicitly included in MD simulations, reduction reactions are based simply on the geometry of the reactant molecule and charge transfer is represented by changing the partial atomic charges to the product ones. Since it is easy to satisfy the geometry constraint in this case, reductive processes could occur spontaneously. To slow down this process, reactions involving a "free" electron are given a lower probability to occur and/or a longer period between between templates checking.

In order to neutralize the whole system after the electrolyte solvents or lithium salts are reduced, the same number of Li^+ cations as that of virtually injected electrons are placed at the electrode−electrolyte interface (nonreactive side) on the next time step after a reaction occurs. This does not affect significantly the pressure of the system. However, every time atoms are inserted a 20 fs NVT run with no reactions is performed to equilibrate the system before returning to the reaction scheme.

All of the reactions implemented happen on a much faster time-scale than they would in reality since our reaction rates are on the order of 1 if a reaction template is satisfied. With this acceleration, we can quickly end up with a deficiency in lithium ions needed to feed the reactions that lead to SEI, due to the slow diffusion of lithium ions in the electrolyte (see Supporting Information). To avoid stalling the reactions, we

https://doi.org/10.1021/acs.jpcc.1c04149
J. Phys. Chem. C XXXX, XXX, XXX−XXX

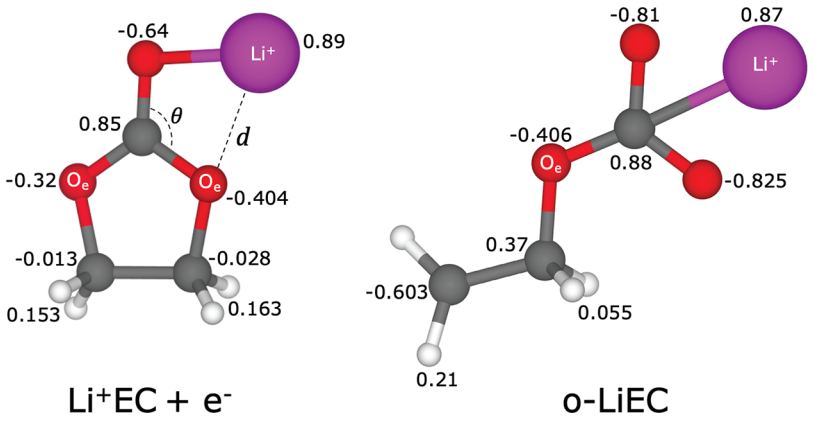

Figure 2. Prereacted (left) and postreacted (right) templates for the one-electron reduction of Li^+(EC). The configuration of a Li^+ coordinated with an EC molecule is used as prereacted topology (left) and the postreacted topology is the ring-opened o−LiEC. The reaction distance cutoff d does not exceed 2.1 Å and the angle θ must measure between 118° and 120° for the reaction to occur. The partial atomic charges of each atom before and after the reaction are shown.

also accelerate the lithium diffusion in the electrolyte to "match" the acceleration in reaction rates. This is done with an external artificial force in the z-direction with magnitude of 0.02 eV/Å acting only on the lithium cations in the electrolyte. We choose this force large enough to increase lithium ion diffusion by an order of magnitude but not too large not to affect the properties of the electrolyte. The radial distribution functions of the Li ions were calculated to verify that the structural properties of the electrolyte were not changed significantly by the external force on Li^+ ions and are available in the Supporting Information.

If a lithium ion does not react in the SEI, it can pass through the silicon, under the influence of an external force in the z-direction and reappear on the electrolyte. This force, we use a value of 4.3 eV/Å, will ensure that lithium ions do not get trapped in the silicon cages and quickly return to the electrolyte.[51] It is only active within 1.2 Å from the anode and drives lithium ions into the anode when they get close to it. In the vicinity of the anode, it can be interpreted as a classical substitute to the chemical force that would lithiate the silicon.

2.2.1. Reductive Dissociation of EC and Their Implementations. In this section, we describe with more details the reactions involving the reductive process of ethylene carbonate solvents. These reactions were introduced based on the reported experimental data and theoretical studies. The first-principles data used for each EC solvent reaction described here and their reactants and products was obtained from the lithium-ion battery electrolyte (LIBE) data set described in ref 52. Note that to be able to use reactants and products in the REACTER protocol in LAMMPS, some artificial covalent bonds in the templates had to be created in the force-field parametrization. Our reaction scheme centers on the reduction mechanism of ethylene carbonate molecules and the formation of three expected SEI components: an inorganic product Li_2CO_3 and two organic lithium bicarbonate compounds, $(ROCO_2Li)_2$ (R = CH_2, CH_2CH_2). Studies using DFT calculations[12,13,44,45] have predicted reaction pathways and confirmed the formation of the latter products. Some specific reaction pathways to LEDC obtained using a reaction network approach have been included.[53]

To onset the reduction process, the first reaction captures a Li^+ coordinated solvent configuration Li^+(EC) by identifying when a Li^+ ion coordinates with a carbonyl oxygen (Oc) of a EC solvent molecule within a distance less than 1.85 Å. The postreacted topology includes a created Li^+−Oc bond to make it a single "molecule" to be used in the next reaction. We make this artificial bond soft enough not to affect the dynamics. We consider this reaction reversible, such that when the Li^+ ion coordinating moves further from the solvent molecule, the bond can break and all atom types revert to the initial ones.

Since EC preferentially coordinates to Li^+ cations, this reaction is often found in our simulations so a check for a new reaction site is performed only every 400 MD timesteps and the probability was set to 0.4. Often this Li^+(EC) complex is short-lived. These parameters allowed us to reduce the potential reactive sites and yet accelerate the reaction rates. In order to favor the reversibility, while allowing some Li^+(EC) complex to survive longer and potentially react further, a probability of 0.6 is set for the Li^+(EC) → Li^+ + EC reaction, while performing a template matching check every 400 timesteps.

Li^+(EC) molecules can undergo to one-electron reduction (see Figure 2 for reaction templates). This redox process can only occur if the reaction site atoms are contained within the artificial redox region and the distance between the Li^+ cation and an ether oxygen (Oe) in the EC does not exceed the reaction distance cutoff. An angle constraint between a carbonyl oxygen, carbonyl carbon, and ether oxygen must be satisfied as well. This will ensure that the Li^+(EC) geometry is ready for the C−Oe bond-breaking to form a ring-opened complex o-LiEC. We found that checking for a potential reactant configuration only every 200 timesteps and lower the probability to 0.4 was necessary to leave some Li^+(EC) available to react with $LiCO_3^-$ to generate Li_2EDC (last reaction in Table 1).

After the formation of o-LiEC molecules, three different pathways can follow: (i) A second reduction of the complex to form the negative charged molecule o−LiEC$^-$; (ii) the direct combination of two o-LiEC to form dilithium butylene dicarbonate $(CH_2CH_2OCO_2Li)_2$, or (iii) the formation of dilithium ethylene dicarbonate $(CH_2OCO_2Li)_2$, the most common found product experimentally[46,54] and usually considered as a dominant SEI component, and a gas molecule via combination of two o-LiEC. For the second reduction, a lower probability and larger frequency than other reactions has

https://doi.org/10.1021/acs.jpcc.1c04149
J. Phys. Chem. C XXXX, XXX, XXX−XXX

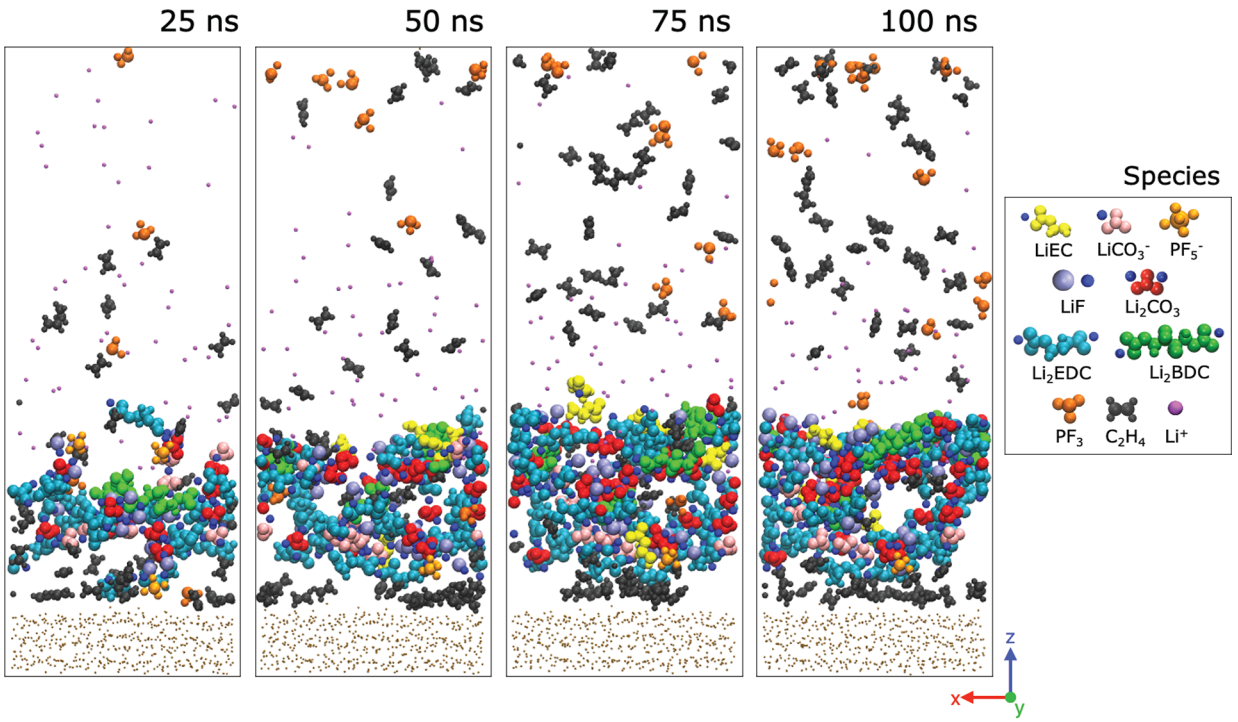

Figure 3. SEI film formation process in the EC-based electrolyte. Snapshots of the reaction products during 100 ns, shown every 25 ns. For visualization purposes, bulk EC and PF_6^- anions are not shown. Li^+ that have not been involved in any reaction are colored in magenta.

been assigned. In such a manner, this reaction does not consume all of the products of the first reduction reaction as soon as they are formed since it is simply based on the geometry and location of the reactant molecule in the simulation box. Without these modifications, the formation of LEDC and LBDC by combination of two ring-opened EC radicals could indeed never occur due to a lack of o-LiEC. The combination of two ring-opened EC radicals has been proposed as a potential reaction mechanism to form these molecules.[13,50]

As proposed in multiple studies,[13] we split the two-electron reduction path of Li^+(EC)

$$EC + 2e^- + Li^+ \rightarrow LiCO_3^- + C_2H_4\uparrow$$

into two reactions: a second reduction on the o-LiEC molecule and a time delayed bond-breaking, implemented though a less frequent check for reactants matching, by which a ethylene gas and an unpaired nucleophilic carbonate anion ($LiCO_3^-$) are generated.

The reaction o-$LiEC^-$ → $LiCO_3^-$ + C_2H_4 effectively should occur spontaneously once the o-$LiEC^-$ are formed. In our simulations, the o-$LiEC^-$ is formed near the anode (as required for a reduction) and rapidly undergoes the bond breaking to create two products, $LiCO_3^-$ and a gas molecule. As the o-$LiEC^-$ molecules do not have time to diffuse in the SEI before the bond breaking, we implemented a time delay by checking a possible reaction every 2000 timesteps, giving time to some of these molecules to move away from the anode. This reduces gas trapping between the anode and the SEI, since we do not expect gas buildup at the anode, a side effect of the acceleration.

Once the carbonate anion ($LiCO_3^-$) is formed, two possible further reaction pathways are implemented: it may react with another Li^+(EC) to form lithium ethylene dicarbonate (LEDC) or be paired with Li^+ to precipitate as insoluble inorganic lithium carbonate Li_2CO_3.

2.2.2. Salt Decomposition. Several theoretical and experimental studies have discussed the decomposition of PF_6^- anion, dissociated from the $LiPF_6$ salt, in EC-based electrolytes, suggesting possible reduction pathways, some of which involve water traces present in the electrolyte.[16,18,41,55,56]

Our reaction scheme includes the PF_6^- decomposition reaction mechanism proposed by Aurbach et al.[41] to form a gaseous PF_3 molecule and three LiF complexes

$$PF_6^- + 3Li^+ + 2e^- \rightarrow 3LiF\downarrow + PF_3$$

Note that reaction has also been implemented in the hybrid MC/MD reaction method done by Takenaka et al.[36] However, due to the complexity of the reaction which requires a very unlikely configuration with an anion surrounded by three Li^+ ions simultaneously at the right place and two electrons, along with the limitations of the REACTER algorithm, we have chosen to split the reaction into three consecutive reaction steps as shown in Table 1.

The reaction mechanism follows two reduction reactions and three Li^+ cations binding to form three LiF: (i) A Li^+ binds with a fluorine atom in the PF_6^- anion creating a LiF and a virtually injected electron forms a PF_5^- molecule. Since this reaction requires an electron, it must occur near the anode surface in the defined redox region. Also, since it competes for Li^+ with the first EC reduction mechanism, we use the same period of 200 steps to check a reaction. On the other hand, we kept a probability of 1 since PF_6^- anions are fewer than EC molecules. (ii) A reduction on the PF_5^- molecule and a second Li^+ cation binds with any F atom to form PF_4^- + LiF, and (iii) a fluorine atom from the PF_4^- molecule bonds with a third Li^+ to reach the final products.

2.3. Computational Details. The bonded interactions (bonds, angles, dihedrals, and impropers) were modeled as

https://doi.org/10.1021/acs.jpcc.1c04149
J. Phys. Chem. C XXXX, XXX, XXX−XXX

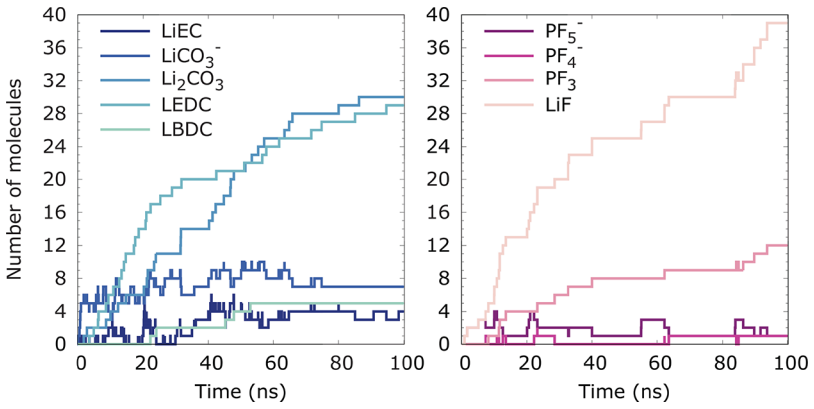

Figure 4. Evolution of reaction product counts during the 100 ns simulation.

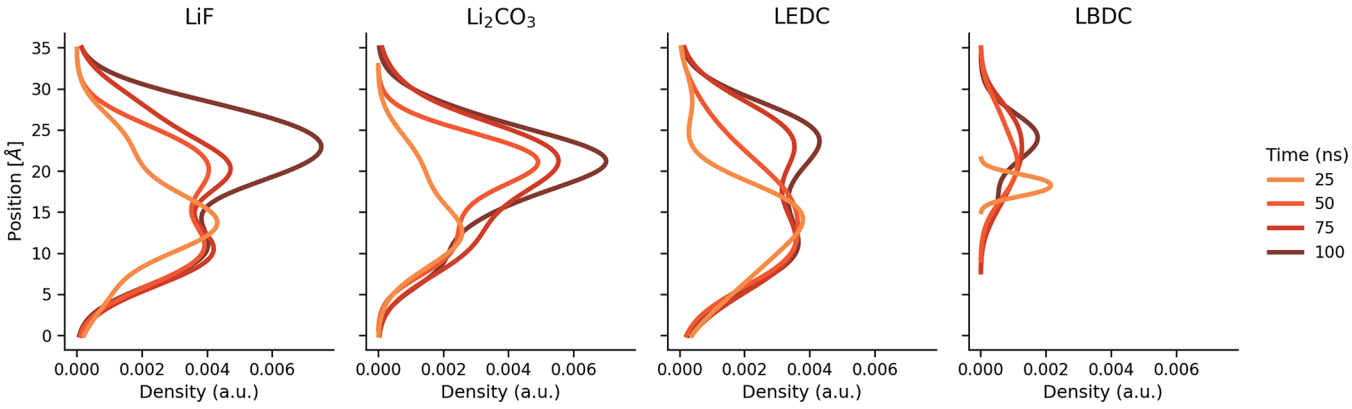

Figure 5. Density distributions of the product components (SEI film) in the present atomistic reaction simulations. The origin of the *z*-coordinate is taken at the position of the silicon atoms on the anode surface in contact with the electrolyte.

harmonic functions and the nonbonded included van der Waals interactions and Coulombic forces. Silicon anode interactions were modeled with the Stillinger–Weber (SW) potential.[57] Nonbonded interactions between amorphous silicon and electrolyte–SEI molecules were modeled by a simple Lennard-Jones potential. The bonded and nonbonded parameters for the electrolyte and SEI molecules were obtained from the nonpolarizable force field OPLS-AA,[58] the PF_6^- anion from Lopes et al.,[59] and the parameters for the Li^+ and F^- ions were taken from Jensen et al.[60]

The partial atomic charges for the electrolyte molecules EC, PF_6^-, and Li^+ were obtained by a full domain DFT calculation with our initial system and the RESP method[61] at the PBE/DVZP level of theory using the CP2K[62] package, and averaging charges for each atomic species. The geometries and partial charges for all EC reaction species were obtained from the LIBE data set.[52] These were calculated using the ωB97X-V/def2-TZVPPD/SMD DFT level of theory but were verified to give consistent charges compared to RESP in CP2K. Geometries and partial charges for the molecules in the PF_6^- decomposition reactions were calculated in CP2K at the PBE/DVZP level of theory.

The particle–particle particle-mesh (PPPM) method was applied to compute long-range Coulombic interactions. A cutoff distance of 12 Å was used for electrostatic interactions. A 12-6 Lennard-Jones potential was used for the van der Waals interactions. Production runs were carried out in the canonical (NVT) ensemble at 298 K using the Nose–Hoover thermostat with a MD time step of 1 fs.

3. RESULTS AND DISCUSSION

We examined the formation processes of the SEI film on the anode surface via MD reaction simulations using the parameters described in the methodology. Figure 3 shows snapshots of the SEI reaction products, displaying how the electrolyte solution develops into the SEI film and gases during an MD reaction simulation up to 100 ns. Throughout the MD simulation o-LiEC complexes (yellow for EC and blue for Li^+ atoms) are constantly produced via reduction of EC solvent molecules on the anode surface as described in Section 2.2.1. If single electron reduced species stay near the silicon surface long enough, they undergo a second reduction reaction forming o-$LiEC^-$ molecules, by dissociation the later ones generate ethylene gases (black) and $LiCO_3^-$ complexes (pink). At the same time, LiEC complexes can form Li_2EDC and Li_2BDC (cyan and green) via their radical polymerization. In our reaction scheme, $LiCO_3^-$ molecules can either form Li_2EDC (cyan) or the inorganic compound Li_2CO_3 (red). Additionally, it is also shown that some PF_6^- anions are reduced to form PF_3 gases (orange) and LiF complexes (F^- colored in light purple and Li^+ cations in blue).

During the early stages, most of the produced open-ring LiEC complexes experience a second electron reduction as shown in Figure 4, where the production of o-LiEC and further evolution and dissociation into $LiCO_3^-$ is constant. Throughout the first nanoseconds, most of the $LiCO_3^-$ complexes react to form Li_2EDC followed by the formation of lithium carbonate Li_2CO_3. We found that about 88% of the Li_2EDC molecules were produced from the two-electron transfer

https://doi.org/10.1021/acs.jpcc.1c04149
J. Phys. Chem. C XXXX, XXX, XXX–XXX

reduction mechanism. This is in agreement with previous studies,[12,63] in which two-electron transfer reduction reactions are faster than the one-electron EC reduction. LiF and Li_2EDC are the predominant species of the initially formed SEI, according to our simulations. As the simulation continues, between 25 and 50 ns, the production of Li_2EDC slows down, whereas the formation of Li_2CO_3 increases continuously up to 60 ns. Consistent with the idea that Li_2EDC is likely to form at a high EC concentration, while Li_2CO_3 tends to form at a low EC concentration.[13] During the last 50 ns, the production of EC decomposition products slows down significantly, the formation of $LiCO_3^-$ stops after 80 ns, since most of the o-LiEC complexes have moved far away from the redox region impeding their further reduction. In the outer regions of the SEI, LiEC produces lithium ethylene dicarbonate and a ethylene gas (C_2H_4) via a dimerization process.

As it can be observed from Figure 4, LiF formation increases again rapidly after 80 ns. This is partially due to reaction of PF_5^- and PF_4^- molecules (both in light orange in Figure 3) that have remained unreacted for long periods of time.

The SEI film at 100 ns is rather homogeneous in composition and does not display a clear double-layer structure. While the relatively short time scales of our simulations prevent us from observing an inorganic core and organic outer layer, we nonetheless observe structural trends that are consistent with the two-layer Peled model.[64] Figure 5 shows the density of the reaction products as a function of time. It is interesting to notice that at early stages the compounds LiF and Li_2EDC are more abundant near the anode surface, consistent with the interpretation of experimental results.[48,65,66] It is also interesting to notice that at longer time scales, these complexes were distributed rather widely and diffusely over in the whole SEI film. The Li_2EDC molecules formed via dimerization (mostly after 75 ns of simulation) are mainly located on the outer SEI, in concurrence with the idea that organic complexes lay farther away from the anode. This is observed as well with Li_2BDC molecules, which start forming as LiEC complexes diffuse in the SEI, away from the anode to finally distribute on the outer SEI. Li_2CO_3 molecules tend to concentrate at the inner part of the SEI initially but later diffuse and mostly aggregate in the middle.

A final note about the presence of C_2H_4 in our simulations. We know that in experiments, gas is produced and released during the SEI growth. We could mimic its release by taking C_2H_4 out of our simulations cells, however we never reached the point where gas molecules agglomerate into bubbles. In addition, we do not want to assume that these molecules do not get trapped into the SEI or at least temporarily affect its growth. Finally, removing the gas molecules could change the density of the system. On the basis of this, we decided to keep the gas molecules in our simulations.

4. CONCLUSIONS

Time-scale is a major challenge when simulating SEI formation at the atomistic level. With recent advances in computer hardware, larger all-atom simulations can be carried out but reducing time-to-solution for each time-step is more challenging with the end of Moore's law and the sequential nature of time. The approach described in this paper shows a way of accelerating the sequence of reactions by essentially associating artificially high reaction rates to each reaction, and making these reactions happen as soon as an appropriate reactants geometry is reached. We have established a set of parameters that lead to simulation results consistent with the current conjectures. We are aware that the results can be affected by these choices however this gives us a baseline for further studies. Indeed, the proposed computational approach can also be applied to investigate relative effects such as the impact of additives in the electrolyte on the initial SEI formation, giving helpful insights on how it could impact its evolution and growth. One limitation is obviously to have a good knowledge of all the reactions involved, either through first-principles simulations or experiments — and there is certainly room for improvement in this direction. Another limitation of our simulations is that, even with 100 ns of MD and an artificially high rate of reactions, we are far away from a fully formed SEI microstructure. However, capturing the behavior at this initial stage is important to set the conditions for more extended modeling, particularly on the mesoscale, where longer time scales can be reached.

■ ASSOCIATED CONTENT

Supporting Information

The Supporting Information is available free of charge at https://pubs.acs.org/doi/10.1021/acs.jpcc.1c04149.

Visualization of reaction templates (reactants and products) with respective reaction cutoffs and constraints. For all species involved in the PF_6^- decomposition, the atomic coordinates, and partial atomic charges are included. The continuum diffusion analysis at atomistic scale and RDF plot for Li^+ under external force (PDF)

■ AUTHOR INFORMATION

Corresponding Author

Lorena Alzate-Vargas − *Computational Sciences and Engineering Division, Oak Ridge National Laboratory, Oak Ridge, Tennessee 37831, United States;* orcid.org/0000-0002-4223-4046; Email: alzatevargll@ornl.gov

Authors

Samuel M. Blau − *Energy Technologies Area, Lawrence Berkeley National Laboratory, Berkeley, California 94720, United States;* orcid.org/0000-0003-3132-3032

Evan Walter Clark Spotte-Smith − *Department of Materials Science and Engineering, University of California, Berkeley, California 94720, United States; Materials Science Division, Lawrence Berkeley National Laboratory, Berkeley, California 94720, United States;* orcid.org/0000-0003-1554-197X

Srikanth Allu − *Computational Sciences and Engineering Division, Oak Ridge National Laboratory, Oak Ridge, Tennessee 37831, United States*

Kristin A. Persson − *Department of Materials Science and Engineering, University of California, Berkeley, California 94720, United States; Molecular Foundry, Lawrence Berkeley National Laboratory, Berkeley, California 94720, United States;* orcid.org/0000-0003-2495-5509

Jean-Luc Fattebert − *Computational Sciences and Engineering Division, Oak Ridge National Laboratory, Oak Ridge, Tennessee 37831, United States*

Complete contact information is available at: https://pubs.acs.org/10.1021/acs.jpcc.1c04149

Notes

The authors declare no competing financial interest.

■ ACKNOWLEDGMENTS

This work is supported by the U.S. Department of Energy Vehicle Technologies Office and was carried out at Oak Ridge National Laboratory under Contract No. DE-AC05-00OR22725 with UT Battelle, LLC. This research used resources of the Compute and Data Environment for Science (CADES) at the Oak Ridge National Laboratory, which is supported by the Office of Science of the U.S. Department of Energy under Contract No. DE-AC05-00OR22725. We gratefully acknowledge Hetal D. Patel and Kara D. Fong for the fruitful discussion.

■ REFERENCES

(1) Armand, M.; Tarascon, J.-M. Building better batteries. *Nature* **2008**, *451*, 652−657.
(2) Goodenough, J. B.; Kim, Y. Challenges for rechargeable Li batteries. *Chem. Mater.* **2010**, *22*, 587−603.
(3) Aurbach, D. Review of selected electrode-solution interactions which determine the performance of Li and Li ion batteries. *J. Power Sources* **2000**, *89*, 206−218.
(4) Xu, K. Nonaqueous liquid electrolytes for lithium-based rechargeable batteries. *Chem. Rev.* **2004**, *104*, 4303−4417.
(5) Agubra, V. A.; Fergus, J. W. The formation and stability of the solid electrolyte interface on the graphite anode. *J. Power Sources* **2014**, *268*, 153−162.
(6) Nie, M.; Abraham, D. P.; Chen, Y.; Bose, A.; Lucht, B. L. Silicon solid electrolyte interphase (SEI) of lithium ion battery characterized by microscopy and spectroscopy. *J. Phys. Chem. C* **2013**, *117*, 13403−13412.
(7) Peled, E.; Menkin, S. Review - SEI: Past, present and future. *J. Electrochem. Soc.* **2017**, *164*, A1703.
(8) Cresce, A. V.; Russell, S. M.; Baker, D. R.; Gaskell, K. J.; Xu, K. In situ and quantitative characterization of solid electrolyte interphases. *Nano Lett.* **2014**, *14*, 1405−1412.
(9) Zheng, J.; Zheng, H.; Wang, R.; Ben, L.; Lu, W.; Chen, L.; Chen, L.; Li, H. 3D visualization of inhomogeneous multi-layered structure and Young's modulus of the solid electrolyte interphase (SEI) on silicon anodes for lithium ion batteries. *Phys. Chem. Chem. Phys.* **2014**, *16*, 13229−13238.
(10) Soto, F. A.; Martinez de la Hoz, J. M.; Seminario, J. M.; Balbuena, P. B. Modeling solid-electrolyte interfacial phenomena in silicon anodes. *Curr. Opin. Chem. Eng.* **2016**, *13*, 179−185.
(11) Wang, A.; Kadam, S.; Li, H.; Shi, S.; Qi, Y. Review on modeling of the anode solid electrolyte interphase (SEI) for lithium-ion batteries. *npj* **2018**, *4*, 15 DOI: 10.1038/s41524-018-0064-0.
(12) Li, T.; Balbuena, P. B. Theoretical studies of the reduction of ethylene carbonate. *Chem. Phys. Lett.* **2000**, *317*, 421−429.
(13) Wang, Y.; Nakamura, S.; Ue, M.; Balbuena, P. B. Theoretical studies to understand surface chemistry on carbon anodes for lithium-ion batteries: Reduction mechanisms of ethylene carbonate. *J. Am. Chem. Soc.* **2001**, *123*, 11708−11718.
(14) Lin, Y.; Jiang, J.; Zhang, Y.; He, X.; Ren, J.; He, P.; Pang, C.; Xiao, C.; Yang, D.; Du, N. Promoting Effect of Si−OH on the Decomposition of Electrolytes in Lithium-Ion Batteries. *Chem. Mater.* **2020**, *32*, 6365−6373.
(15) Leung, K.; Budzien, J. L. Ab initio molecular dynamics simulations of the initial stages of solid-electrolyte interphase formation on lithium ion battery graphitic anodes. *Phys. Chem. Chem. Phys.* **2010**, *12*, 6583−6586.
(16) Ganesh, P.; Kent, P. R.; Jiang, D. E. Solid-electrolyte interphase formation and electrolyte reduction at Li-Ion battery graphite anodes: Insights from first-principles molecular dynamics. *J. Phys. Chem. C* **2012**, *116*, 24476−24481.
(17) Martinez de la Hoz, J. M.; Leung, K.; Balbuena, P. B. Reduction mechanisms of ethylene carbonate on si anodes of lithium-ion batteries: Effects of degree of lithiation and nature of exposed surface. *ACS Appl. Mater. Interfaces* **2013**, *5*, 13457−13465.
(18) Leung, K. Predicting the voltage dependence of interfacial electrochemical processes at lithium-intercalated graphite edge planes. *Phys. Chem. Chem. Phys.* **2015**, *17*, 1637−1643.
(19) Martinez de la Hoz, J. M.; Soto, F. A.; Balbuena, P. B. Effect of the Electrolyte Composition on SEI Reactions at Si Anodes of Li-Ion Batteries. *J. Phys. Chem. C* **2015**, *119*, 7060−7068.
(20) Hankins, K.; Soto, F. A.; Balbuena, P. B. Insights into the Li Intercalation and SEI Formation on LiSi Nanoclusters. *J. Electrochem. Soc.* **2017**, *164*, E3457−E3464.
(21) Tasaki, K. Computational Study of Salt Association in Li-Ion Battery Electrolyte. *J. Electrochem. Soc.* **2002**, *149*, A418.
(22) Kumar, N.; Seminario, J. M. Lithium-ion model behavior in an ethylene carbonate electrolyte using molecular dynamics. *J. Phys. Chem. C* **2016**, *120*, 16322−16332.
(23) Bedrov, D.; Borodin, O.; Hooper, J. B. Li+ Transport and Mechanical Properties of Model Solid Electrolyte Interphases (SEI): Insight from Atomistic Molecular Dynamics Simulations. *J. Phys. Chem. C* **2017**, *121*, 16098−16109.
(24) Muralidharan, A.; Chaudhari, M. I.; Pratt, L. R.; Rempe, S. B. Molecular Dynamics of Lithium Ion Transport in a Model Solid Electrolyte Interphase. *Sci. Rep.* **2018**, *8*, 10736.
(25) Hou, T.; Yang, G.; Rajput, N. N.; Self, J.; Park, S. W.; Nanda, J.; Persson, K. A. The influence of FEC on the solvation structure and reduction reaction of LiPF6/EC electrolytes and its implication for solid electrolyte interphase formation. *Nano Energy* **2019**, *64*, 103881.
(26) Borodin, O.; Zhuang, G. V.; Ross, P. N.; Xu, K. Molecular dynamics simulations and experimental study of lithium ion transport in dilithium ethylene dicarbonate. *J. Phys. Chem. C* **2013**, *117*, 7433−7444.
(27) Ebrahiminia, M.; Hooper, J. B.; Bedrov, D. Structural, mechanical, and dynamical properties of amorphous Li2CO3 from molecular dynamics simulations. *Crystals* **2018**, *8*, 473.
(28) Jorn, R.; Kumar, R.; Abraham, D. P.; Voth, G. A. Atomistic modeling of the electrode-electrolyte interface in Li-ion energy storage systems: Electrolyte structuring. *J. Phys. Chem. C* **2013**, *117*, 3747−3761.
(29) Raguette, L.; Jorn, R. Ion Solvation and Dynamics at Solid Electrolyte Interphases: A Long Way from Bulk? *J. Phys. Chem. C* **2018**, *122*, 3219−3232.
(30) Boyer, M. J.; Hwang, G. S. Molecular dynamics investigation of reduced ethylene carbonate aggregation at the onset of solid electrolyte interphase formation. *Phys. Chem. Chem. Phys.* **2019**, *21*, 22449−22455.
(31) Borodin, O.; Smith, G. D. Quantum chemistry and molecular dynamics simulation study of dimethyl carbonate: Ethylene carbonate electrolytes doped with LiPF6. *J. Phys. Chem. B* **2009**, *113*, 1763−1776.
(32) Wang, Y.; Liu, Y.; Tu, Y.; Wang, Q. Reductive Decomposition of Solvents and Additives toward Solid-Electrolyte Interphase Formation in Lithium-Ion Battery. *J. Phys. Chem. C* **2020**, *124*, 9099−9108.
(33) Kim, S. P.; Duin, A. C.; Shenoy, V. B. Effect of electrolytes on the structure and evolution of the solid electrolyte interphase (SEI) in Li-ion batteries: A molecular dynamics study. *J. Power Sources* **2011**, *196*, 8590−8597.
(34) Yun, K. S.; Pai, S. J.; Yeo, B. C.; Lee, K. R.; Kim, S. J.; Han, S. S. Simulation Protocol for Prediction of a Solid-Electrolyte Interphase on the Silicon-based Anodes of a Lithium-Ion Battery: ReaxFF Reactive Force Field. *J. Phys. Chem. Lett.* **2017**, *8*, 2812−2818.
(35) Bertolini, S.; Balbuena, P. B. Buildup of the Solid Electrolyte Interphase on Lithium-Metal Anodes: Reactive Molecular Dynamics Study. *J. Phys. Chem. C* **2018**, *122*, 10783−10791.
(36) Takenaka, N.; Suzuki, Y.; Sakai, H.; Nagaoka, M. On electrolyte-dependent formation of solid electrolyte interphase film in lithium-ion batteries: Strong sensitivity to small structural

difference of electrolyte molecules. *J. Phys. Chem. C* **2014**, *118*, 10874−10882.
(37) Gissinger, J. R.; Jensen, B. D.; Wise, K. E. Modeling chemical reactions in classical molecular dynamics simulations. *Polymer* **2017**, *128*, 211−217.
(38) Gissinger, J. R.; Jensen, B. D.; Wise, K. E. Reacter: A heuristic method for reactive molecular dynamics. *Macromolecules* **2020**, *53*, 9953−9961.
(39) Martínez, L.; Andrade, R.; Birgin, E. G.; Martínez, J. M. PACKMOL: A package for building initial configurations for molecular dynamics simulations. *J. Comput. Chem.* **2009**, *30*, 2157−2164.
(40) Plimpton, S. Fast Parallel Algorithms for Short-Range Molecular Dynamics. *J. Comput. Phys.* **1995**, *117*, 1−19.
(41) Aurbach, D.; Markovsky, B.; Shechter, A.; Ein-Eli, Y.; Cohen, H. A Comparative Study of Synthetic Graphite and Li Electrodes in Electrolyte Solutions Based on Ethylene Carbonate-Dimethyl Carbonate Mixtures. *J. Electrochem. Soc.* **1996**, *143*, 3809−3820.
(42) Aurbach, D.; Levi, M. D.; Levi, E.; Schechter, A. Failure and Stabilization Mechanisms of Graphite Electrodes. *J. Phys. Chem. B* **1997**, *101*, 2195−2206.
(43) Islam, M. M.; van Duin, A. C. Reductive Decomposition Reactions of Ethylene Carbonate by Explicit Electron Transfer from Lithium: An eReaxFF Molecular Dynamics Study. *J. Phys. Chem. C* **2016**, *120*, 27128−27134.
(44) Burkhardt, S. E. Impact of Chemical Follow-up Reactions for Lithium Ion Electrolytes: Generation of Nucleophilic Species, Solid Electrolyte Interphase, and Gas Formation. *J. Electrochem. Soc.* **2017**, *164*, A684−A690.
(45) Liu, X.; Zhou, J.; Xu, Z.; Wang, Y. Atomic thermodynamics and microkinetics of the reduction mechanism of electrolyte additives to facilitate the formation of solid electrolyte interphases in lithium-ion batteries. *RSC Adv.* **2020**, *10*, 16302−16312.
(46) Zhuang, G. V.; Xu, K.; Yang, H.; Jow, T. R.; Ross, P. N. Lithium ethylene dicarbonate identified as the primary product of chemical and electrochemical reduction of EC in 1.2 M LiPF 6/EC:EMC electrolyte. *J. Phys. Chem. B* **2005**, *109*, 17567−17573.
(47) Pereira-Nabais, C.; Świątowska, J.; Chagnes, A.; Gohier, A.; Zanna, S.; Seyeux, A.; Tran-Van, P.; Cojocaru, C. S.; Cassir, M.; Marcus, P. Insight into the solid electrolyte interphase on Si nanowires in lithium-ion battery: Chemical and morphological modifications upon cycling. *J. Phys. Chem. C* **2014**, *118*, 2919−2928.
(48) Young, B. T.; Heskett, D. R.; Nguyen, C. C.; Nie, M.; Woicik, J. C.; Lucht, B. L. Hard X-ray photoelectron spectroscopy (HAXPES) investigation of the silicon solid electrolyte interphase (SEI) in lithium-ion batteries. *ACS Appl. Mater. Interfaces* **2015**, *7*, 20004−20011.
(49) Jin, Y.; Kneusels, N. J. H.; Magusin, P. C.; Kim, G.; Castillo-Martínez, E.; Marbella, L. E.; Kerber, R. N.; Howe, D. J.; Paul, S.; Liu, T.; et al. Identifying the Structural Basis for the Increased Stability of the Solid Electrolyte Interphase Formed on Silicon with the Additive Fluoroethylene Carbonate. *J. Am. Chem. Soc.* **2017**, *139*, 14992−15004.
(50) Nanda, J.; Yang, G.; Hou, T.; Voylov, D. N.; Li, X.; Ruther, R. E.; Naguib, M.; Persson, K.; Veith, G. M.; Sokolov, A. P. Unraveling the Nanoscale Heterogeneity of Solid Electrolyte Interphase Using Tip-Enhanced Raman Spectroscopy. *Joule* **2019**, *3*, 2001−2019.
(51) Wang, H.; Ji, X.; Chen, C.; Xu, K.; Miao, L. Lithium diffusion in silicon and induced structure disorder: A molecular dynamics study. *AIP Adv.* **2013**, *3*, 112102.
(52) Spotte-Smith, E. W. C.; Blau, S.; Xie, X.; Patel, H.; Wen, M.; Wood, B.; Dwaraknath, S.; Persson, K. Quantum Chemical Calculations of Lithium-Ion Battery Electrolyte and Interphase Species. *Sci. Data* **2021**, *8*, 203.
(53) Blau, S. M.; Patel, H. D.; Spotte-Smith, E. W. C.; Xie, X.; Dwaraknath, S.; Persson, K. A. A chemically consistent graph architecture for massive reaction networks applied to solid-electrolyte interphase formation. *Chemical Science* **2021**, *12*, 4931.
(54) Heiskanen, S. K.; Kim, J.; Lucht, B. L. Generation and Evolution of the Solid Electrolyte Interphase of Lithium-Ion Batteries. *Joule* **2019**, *3*, 2322−2333.
(55) Bar-Tow, D.; Peled, E.; Burstein, L. A Study of Highly Oriented Pyrolytic Graphite as a Model for the Graphite Anode in Li-Ion Batteries. *J. Electrochem. Soc.* **1999**, *146*, 824−832.
(56) Kawamura, T.; Okada, S.; Yamaki, J.-i. Decomposition reaction of LiPF6-based electrolytes for lithium ion cells. *J. Power Sources* **2006**, *156*, 547−554.
(57) Stillinger, F. H.; Weber, T. A. Computer simulation of local order in condensed phases of silicon. *Phys. Rev. B: Condens. Matter Mater. Phys.* **1985**, *31*, 5262−5271.
(58) Jorgensen, W. L.; Maxwell, D. S.; Tirado-rives, J. Development and Testing of the OPLS All-Atom Force Field on Conformational Energetics and Properties of Organic Liquids. *J. Am. Chem. Soc.* **1996**, *118*, 11225−11236.
(59) Canongia Lopes, J. N.; Padua, A. A. H. Molecular force field for ionic liquids composed of triflate or bistriflylimide anions. *J. Phys. Chem. B* **2004**, *108*, 16893−16898.
(60) Jensen, K. P.; Jorgensen, W. L. Halide, ammonium, and alkali metal ion parameters for modeling aqueous solutions. *J. Chem. Theory Comput.* **2006**, *2*, 1499−1509.
(61) Bayly, C. I.; Cieplak, P.; Cornell, W. D.; Kollman, P. A. A well-behaved electrostatic potential based method using charge restraints for deriving atomic charges: The RESP model. *J. Phys. Chem.* **1993**, *97*, 10269−10280.
(62) Kuhne, T. D.; Iannuzzi, M.; Del Ben, M.; Rybkin, V. V.; Seewald, P.; Stein, F.; Laino, T.; Khaliullin, R. Z.; Schutt, O.; Schiffmann, F.; Golze, D.; Wilhelm, J.; Chulkov, S.; Bani-Hashemian, M. H.; Weber, V.; Borstnik, U.; Taillefumier, M.; Jakobovits, A. S.; Lazzaro, A.; Pabst, H.; Muller, T.; Schade, R.; Guidon, M.; Andermatt, S.; Holmberg, N.; Schenter, G. K.; Hehn, A.; Bussy, A.; Belleflamme, F.; Tabacchi, G.; Gloß, A.; Lass, M.; Bethune, I.; Mundy, C. J.; Plessl, C.; Watkins, M.; VandeVondele, J.; Krack, M.; Hutter, J. CP2K: An electronic structure and molecular dynamics software package -Quickstep: Efficient and accurate electronic structure calculations. *J. Chem. Phys.* **2020**, *152*, 194103.
(63) Leung, K. Two-electron reduction of ethylene carbonate: A quantum chemistry re-examination of mechanisms. *Chem. Phys. Lett.* **2013**, *568*−*569*, 1−8.
(64) Peled, E.; Golodnitsky, D.; Ardel, G. Advanced Model for Solid Electrolyte Interphase Electrodes in Liquid and Polymer Electrolytes. *J. Electrochem. Soc.* **1997**, *144*, L208−L210.
(65) Seo, D. M.; Chalasani, D.; Parimalam, B. S.; Kadam, R.; Nie, M.; Lucht, B. L. Reduction reactions of carbonate solvents for lithium ion batteries. *ECS Electrochem. Lett.* **2014**, *3*, A91−A93.
(66) Kim, J.; Chae, O. B.; Lucht, B. L. Perspective−Structure and Stability of the Solid Electrolyte Interphase on Silicon Anodes of Lithium-ion Batteries. *J. Electrochem. Soc.* **2021**, *168*, 030521.

https://doi.org/10.1021/acs.jpcc.1c04149
J. Phys. Chem. C XXXX, XXX, XXX−XXX